PCCP

ROYAL SOCIETY OF CHEMISTRY

PAPER

View Article Online
View Journal | View Issue

Cite this: *Phys. Chem. Chem. Phys.*, 2023, **25**, 7394

The role of hydration in atmospheric salt particle formation†

Nanna Myllys [ab]

Received 4th January 2023,
Accepted 8th February 2023

DOI: 10.1039/d3cp00049d

rsc.li/pccp

New-particle formation from condensable acid and base molecules is a ubiquitous phenomenon in the atmosphere. The role of water in salt particle formation is not fully understood as it can stabilize or destabilize cluster structures, which leads to non-linear effects on cluster formation dynamics. In the studied systems, increased relative humidity can enhance the particle formation for up to four orders of magnitude in the case of nitric acid, but it can also slightly reduce the particle formation in the cases of sulfuric acid and methanesulfonic acid. As the effect of relative humidity in salt particle formation varies many orders of magnitude depending on the acid and base molecules, neglecting hydration or using the same value for different systems may introduce remarkable inaccuracies in large-scale models.

1 Introduction

Atmospheric salt particles are important in climate control, and climate models suggest that they cause an overall cooling effect.[1,2] The ability of different types of aerosol particles to act as cloud condensation nuclei (CCN) depends on their size and composition.[3–5] Sulfate and sea salt particles have an ability to absorb water, *i.e.*, they are hygroscopic,[6,7] whereas soot and mineral particles cannot act as CCN as they may offer a seed for ice nucleation in colder parts of the atmosphere.[8] As different types of chemical compounds may be mixed within the aerosol particles, the situation is even more complicated, hampering the efforts in developing reliable and predictive climate models.[9]

The properties and amount of CCN affect cloud formation and properties in two major ways: Twomey and Albrecht effects.[10,11] The former refers to the fact that in cloud formation, the water vapor will be distributed among all of the available CCN. The higher the number of CCN, the smaller the growth of water droplets as the water molecules will be distributed among more particles. This leads to more efficient light scattering, *i.e.*, cooling effect. The latter refers to the fact that in clouds that form in the presence of many CCN, the water droplets are smaller and more lightweight, meaning that they are less likely to fall out of the cloud as rain. This increases the lifetime of CCN as well as clouds. These indirect effects of aerosol are poorly understood, thus adequate representation of new-particle formation (NPF) in atmospheric transport models is essential for accurate estimation of ambient CCN numbers.[12]

Temperature and relative humidity (RH) are important but poorly understood parameters in NPF.[13–15] They vary greatly depending on the altitude, latitude, season, and the time of the day. Thus, increased understanding of the effects of RH and temperature on the NPF mechanisms and rates is essential to accurate estimation of the aerosol indirect effects. In our recent study, a general parametrization for salt nanoparticle formation under dry conditions and at atmospherically relevant temperatures has been derived.[16] Here the focus is on the effect of relative humidity on the NPF from acid and base molecules. This is needed to estimate the aerosol number concentration as well as how acid–base particles absorb water vapor which relates their efficiency to act as CCN. Here our model system contains three different acids: sulfuric acid (SA), methanesulfonic acid (MSA), and nitric acid (NA) and one base: guanidine (GUA). Recently SA–GUA and MSA–GUA systems have been shown to lead to efficient particle formation,[17–19] and here NA–GUA clusters are also found to be relatively stable. While the role of hydration in the cases of acids with ammonia or amines has been previously investigated,[20–22] it has not been studied in the case of guanidine. This study shows that hydration effects are highly complicated, but important to understand, in the initial steps of acid–guanidine particle formation.

2 Computational details

Acid–base clusters of sulfuric acid, methanesulfonic acid, and nitric acid with guanidine, up to two acid, two base and four water (W) molecules have been studied using accurate quantum

[a] *Department of Chemistry, University of Helsinki, Helsinki 00014, Finland. E-mail: nanna.myllys@helsinki.fi*
[b] *Institute for Atmospheric and Earth System Research, University of Helsinki, Helsinki 00014, Finland*

† Electronic supplementary information (ESI) available. See DOI: https://doi.org/10.1039/d3cp00049d

chemical methods. To find the global minimum energy cluster structures, the potential energy surface of all the acid–base–water clusters has been explored using a systematic configurational sampling technique.[23] To create the initial cluster structures, 3000 random guesses and 100 exploration loops have been used, with a scout limit of 4 in the ABCluster program,[24,25] and for each building block combination 2000 of the lowest energy structures has been saved and subsequently optimized by the tight-binding method GFN2-*x* TB with a very tight optimization criteria.[26] Based on the electronic energies, radius of gyration, and dipole moments, different conformers have been separated, which were then optimized using the w B97X-D/6-31+G* level of theory.[27,28] Based on the obtained electronic energies, structures with a maximum of N kcal mol^{-1} from the lowest electronic energy (where N is the number of molecules in the cluster) have been identified. For remaining structures, the w B97X-D/6-31++G** level of theory was used for final optimization and vibrational frequency calculation using Gaussian 16 RevA.03.[29] Gibbs free energy structures within 0.5 kcal mol^{-1} from global minimum have been selected (2–5 structures), for which single point energy calculations have been performed using the highly accurate DLPNO–CCSD(T)/aug-cc-pVTZ level of theory with tight pair natural orbital criteria and tight self consistent field criteria as implemented in Orca version 4.2.1.[30–35] For each cluster, the global minimum Gibbs free energy structure at the DLPNO–CCSD(T)/aug-cc-pVTZ//w B97X-D/6-31++G** level has been identified.[36–39] The calculated thermochemical data are further used to study the population dynamics of water clusters using Atmospheric Cluster Dynamics Code (ACDC).[40,41] Thermochemical data, ACDC simulation details, and *xyz* coordinates are available in the ESI.†

3 Results and discussion

3.1 Dry clusters

Acid–guanidine cluster stabilities up to the dry cluster size of four acid and four base molecules have been investigated. Overall evaporation rates at 273 K for guanidine and sulfuric acid, methanesulfonic acid and nitric acid clusters are given in Fig. 1.

Interestingly, the clusters with more GUA than NA molecules have several orders of magnitude lower evaporation rates than those having more NA than GUA molecules. This might be related to the higher vapor pressure of NA (0.083 atm in 298 K) than that of GUA (0.0029 atm in 298 K). However, NA–GUA clusters are stable only in a diagonal axis (equal number of acid and base molecules), meaning that the aerosol particles are likely to be neutral with the NA : GUA ratio of 1 : 1 under atmospherically relevant conditions. Recently, equal acid-to-base ratio has been measured and modeled for nitric acid–dimethylamine particles under dry and humid conditions.[42] Diagonal NA–GUA clusters have very high symmetry as can be seen from Fig. 2. In all clusters, NA has donated its proton to GUA in all clusters and clusters contain a large number of intermolecular interactions.

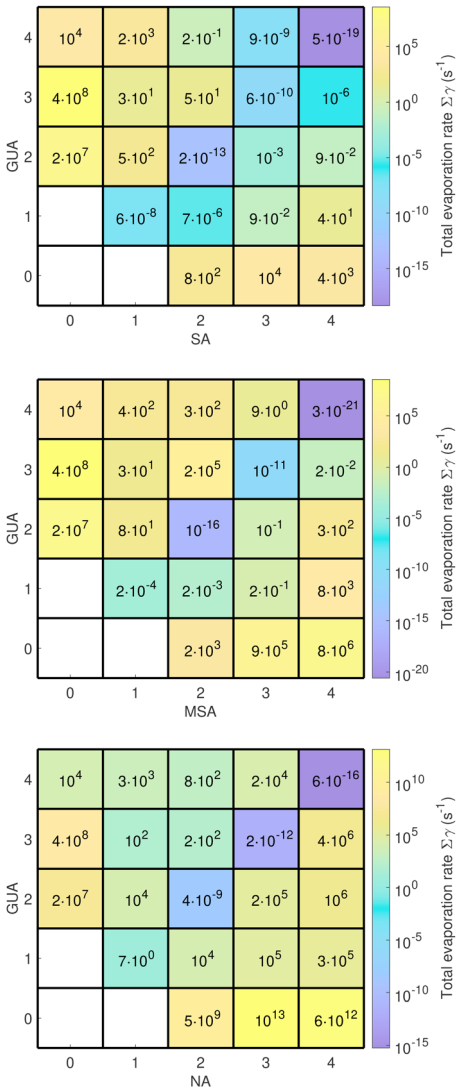

Fig. 1 Total evaporation rates of dry acid–guanidine clusters at 273 K.

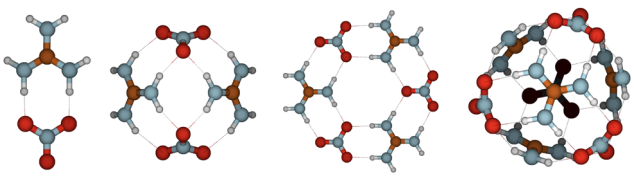

Fig. 2 Molecular structures of diagonal NA–GUA clusters.

As shown earlier, the diagonal SA–GUA clusters do not evaporate under atmospheric conditions.[17] Almost all heteromolecular SA–GUA clusters are relatively stable against evaporation; even those where the number of acid and base molecules differ by two have low evaporation rates. In the case of MSA–GUA, the diagonal clusters are very stable as the structures remind those of SA–GUA clusters: high symmetry and strong ionic bonds between anions and cations. Recently Liu *et al.* built a quantitative structure–activity relationship model and

Table 1 Effect of relative humidity on the evaporation rates. Calculated as an overall evaporation rate of clusters with 0–4 water molecules at RH = 50 or 100% divided by a cluster evaporation rate at RH = 0%. A value <1 implies that water stabilizes the cluster and a value >1 implies that water destabilizes the cluster

RH = 50%	SA	MSA	NA
1acid1GUA	10^{-2}	5×10^{-4}	0.2
1acid2GUA	2.0	12.5	0.1
2acid1GUA	43	90	1.3
2acid2GUA	10^{3}	2×10^{4}	1.3
RH = 100%	**SA**	**MSA**	**NA**
1acid1GUA	2×10^{-2}	5×10^{-5}	2×10^{-2}
1acid2GUA	4.0	62.5	0.3
2acid1GUA	114	200	3.8
2acid2GUA	10^{4}	3×10^{5}	3.3

predicted GUA to form very strong interactions with MSA, and thus be possibly the strongest enhancer in the MSA-driven NPF under atmospheric conditions.[19] Clusters where the number of MSA is greater than GUA molecules are stable, which might be due to the lower vapor pressure of MSA (5.6×10^{-7} atm in 298 K) than that of GUA, and perhaps the volatility of participating monomers could be used as a predictor for non-neutral acid-to-base ratio in salt particles. Thus, under acid-rich conditions, MSA–GUA particles are likely to be acidic. A similar effect has also been observed for MSA particles with methylamine and ammonia.[43]

3.2 Hydration affects the cluster stability

The effect of increased relative humidity to the overall stability of acid–guanidine clusters has been evaluated. As previous studies have found that clusters consisting of sulfuric acid and amines or ammonia are mainly hydrated by a maximum of three water molecules,[20,44,45] four water molecules used in this study can safely be assumed to be more than enough to describe the hydration effect. Additionally, as the clusters consisting of two acid and two guanidine molecules are very stable, to save computational resources, only smallest clusters (up to two acid and two base molecules) are included in the system to investigate the hydration.

The effect of relative humidity on the overall evaporation rates of acid–guanidine clusters has been computed as a ratio of overall evaporation rate of clusters with 0–4 water molecules and evaporation rate of a dry cluster (see Table 1).

Heterodimer stability is known to be a key factor which affects the ability of a cluster to grow to a large aerosol particle.[18,46] Therefore, how water molecules affect the heterodimer stability may have a large impact on the NPF rates.[47] Table 1 shows that acid–guanidine heterodimers are more stable against evaporation at increased relative humidity. However, as dry SA–GUA and MSA–GUA heterodimers have very low evaporation rates (6×10^{-8} and 2×10^{-4} s^{-1}, respectively), additional stabilization for these clusters is likely to have negligible effect on the NPF rates. Earlier studies have shown that for stable acid–base clusters where the role of evaporation is minor, the effect of hydration is usually small.[21] As NA–GUA heterodimers have just medium–low evaporation rate, 7 s^{-1}, the increased relative humidity may intensify the NA–GUA particle formation remarkably. Clusters containing one NA and two GUA molecules are also stabilized under humid conditions, but 1SA2GUA and 1MSA2GUA clusters are slightly less stable at increased relative humidity. Other studied clusters containing two acid and one or two guanidine molecules are destabilized by water molecules. The effect is significant in the case of SA and MSA clusters for up to five orders of magnitude, whereas for NA containing clusters the effect is very small.

3.3 Water may intensify or inhibit clustering

The temperature has a straightforward effect on the NPF rates under atmospheric relevant conditions: the lower the temperature,

Table 2 Computed humidity factors to the particle formation rates, HF_{RH}, at RH = 10, 50, and 100%. NPF rate at RH = 0% is given as J_{dry} [cm^{-3} s^{-1}], and the humidity factor is calculated as J_{humid} divided by J_{dry}. The larger the HF_{RH} the higher the enhancement of relative humidity. $HF_{RH} < 1$ implies that water inhibits the particle formation

	T = 248 K and [GUA] = 10^3 cm^{-3}				T = 273 K and [GUA] = 10^4 cm^{-3}				T = 298 K and [GUA] = 10^5 cm^{-3}			
[Acid] cm^{-3}	J_{dry}	HF_{10}	HF_{50}	HF_{100}	J_{dry}	HF_{10}	HF_{50}	HF_{100}	J_{dry}	HF_{10}	HF_{50}	HF_{100}
[SA]												
10^6	6×10^{-5}	1.5	1.8	1.9	7×10^{-4}	1.3	1.5	1.3	4×10^{-1}	1.1	0.9	0.9
10^7	7×10^{-4}	1.2	1.5	1.6	7×10^{-1}	1.2	1.4	1.5	5×10^{1}	1.1	1	1
10^8	6×10^{-1}	1.2	1.4	1.5	4×10^{1}	1.1	1.3	1.3	10^3	1	1.1	1.1
10^9	4×10^{1}	1.1	1.3	1.3	10^3	1	1.1	1.2	2×10^{4}	1	1.1	1.1
10^{10}	10^3	1	1.1	1.1	10^4	1	1.1	1.1	2×10^{5}	1	1	1.1
[MSA]												
10^6	8×10^{-5}	1.4	1	0.8	3×10^{-4}	1.2	1.1	1.1	10^{-4}	22	272	297
10^7	8×10^{-4}	1.3	1.3	1.2	6×10^{-1}	1.2	1.1	1.1	2×10^{-1}	20	164	174
10^8	7×10^{-1}	1.2	1.3	1.3	5×10^{1}	1.1	1.1	1.1	4×10^{1}	10	29	30
10^9	4×10^{1}	1.1	1.2	1.2	10^3	1	1.1	1.1	9×10^{3}	1.5	1.8	1.9
10^{10}	10^3	1	1.1	1.1	2×10^{4}	1	1	1	2×10^{5}	1	1	1
[NA]												
10^6	6×10^{-10}	1.2	219	8284	4×10^{-11}	1.1	31	1910	9×10^{-12}	1	6.6	239
10^7	10^{-7}	1.2	207	7752	7×10^{-9}	1.1	30	1790	2×10^{-9}	1	6.3	224
10^8	10^{-5}	1.2	205	7568	8×10^{-7}	1.1	29	1767	2×10^{-7}	1	6.2	222
10^9	10^{-4}	1.2	204	6840	8×10^{-5}	1.1	29	1764	2×10^{-5}	1	6.2	221
10^{10}	10^{-1}	1.2	197	3723	8×10^{-4}	1.1	29	1760	2×10^{-4}	1	6.2	221

the higher the NPF rate.[40,48] The effect of hydration on the NPF is more complex. This is because the overall evaporation rate constants can either increase or decrease due to hydration as shown in Table 1, which leads to nonlinear effects on the NPF. For instance, in the case of acid–dimethylamine systems: for SA–DMA particle formation, the effect of RH is negligible,[21] for MSA–DMA particle formation, water is essential,[49] and NA–DMA particle formation rates are only weakly impacted by the increased relative humidity.[42]

The effect of hydration on the NPF rates under various atmospheric conditions has been modeled. Table 2 shows the effect of relative humidity on the acid–guanidine particle formation rate under various atmospherically relevant conditions. Typical concentrations of atmospheric gas phase SA and MSA are in the range of 10^5–10^7 cm^{-3},[50,51] and NA has been detected in concentrations around 10^{10} cm^{-3}.[52,53] It should be noted that J_{dry} might not correspond to the actual NPF rate but the highest limit. This is because the used system size (up to two acid and two base molecules) is not large enough to account for cluster evaporation leading to the overestimation of the particle formation.[54] Therefore, one should focus on the humidity factor, $\mathrm{HF} = \frac{J_{humid}}{J_{dry}}$, rather than absolute J values.

Sulfuric acid and methanesulfonic acid drive the salt particle formation almost at equal rates at 248 and 273 K. The particle formation occurs at the kinetic limit as previously shown for SA–GUA particle formation.[16] Therefore, water vapor cannot intensify NPF. Interestingly, in the case of MSA–GUA at 248 K and RH = 100%, water vapor lowers the NPF rate *ca.* 20% compared to the dry NPF. The possible reason for this is the destabilisation of water molecules of the 2MSA1GUA cluster, which inhibits the cluster formation *via* that cluster. The overall evaporation rate of the hydrated 2MSA1GUA cluster at 248 K is 300 times higher than that of a dry one. At 298 K water vapor can increase MSA–GUA particle formation for up to 300 times, but under the same conditions, it has a small decreasing effect to the SA–GUA particle formation. At 298 K, the 2SA1GUA cluster is 50 times less stable at RH = 100% than at RH = 0%, which may cause a small reduction in the NPF process.

Nitric acid–guanidine particle formation has several orders of magnitude lower formation rate which is due to the fact that the small NA–GUA clusters may evaporate under simulation conditions. Thus, the stabilisation effect of the NA–GUA heterodimer by water molecules has a significant role in the initial steps of nitric acid NPF. The high relative humidity increases the NPF rate by up to 8000 times. As nitric acid is ubiquitous throughout the atmosphere, typically present in low $\mathrm{ppb_V}$ concentrations, significantly enhanced NPF rates at high RH may affect the properties and concentration of cloud condensation nuclei in the atmosphere, thus the Earth's radiation balance.[55,56]

3.4 Salt particle hydration

Atmospheric aerosol particles may absorb water vapor, which affects their structure and properties. Salt particle hydration has been simulated and Fig. 3 shows the hydration distributions of acid–guanidine clusters up to the size of two acid, two base and four water molecules at 248 K at RH = 10%.

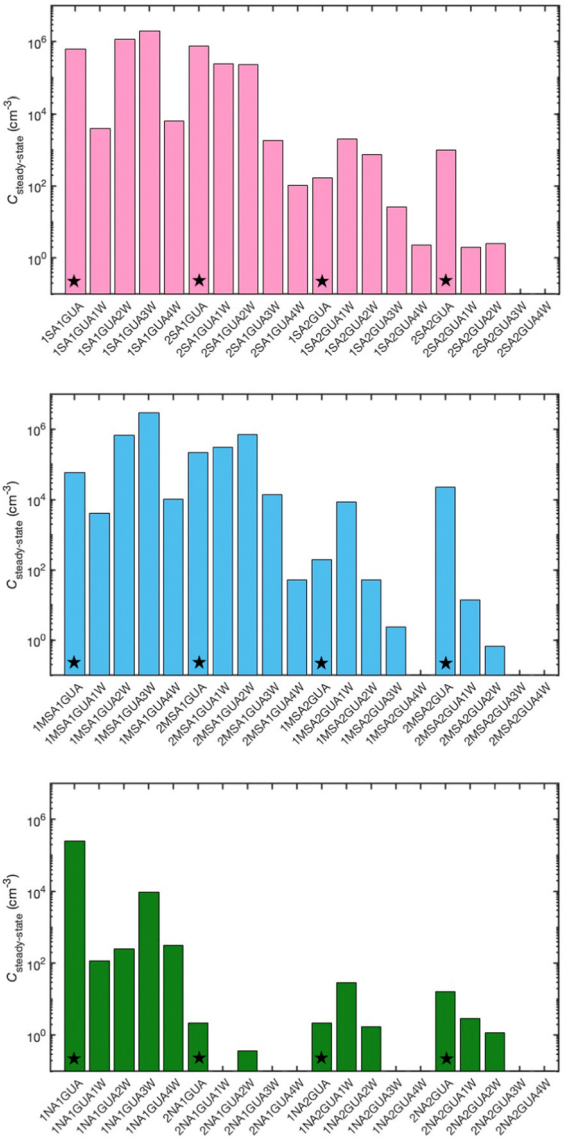

Fig. 3 Hydration distribution of acid–guanidine clusters at 248 K, RH = 10%, [acid] = [guanidine] = 10^7 cm^{-3}. Dry clusters are marked by stars.

Many acid–guanidine clusters seem to exist in higher equilibrium concentration in hydrated than bare form. In particular, in the case of 1MSA1GUA, the extent of dry cluster is less than 1% of the total 1MSA1GUA*n* W concentration. SA–GUA and MSA–GUA clusters have quite similar hydration distributions. It is notable, however, that MSA–GUA clusters have the highest water vapor absorption ability, even though SA can form more hydrogen bonds than MSA. Guanidine and the studied acids form clusters with high water absorption ability, and the order to absorb water vapor is MSA > SA > NA. The result is quite surprising as generally it is believed that the hydration ability is directly linked to the number of hydrogen binding sites.[57–60] Molecular figures showing the hydrogen bond formation for two acid and two guanidine clusters with one to four water molecules are presented in the ESI.†

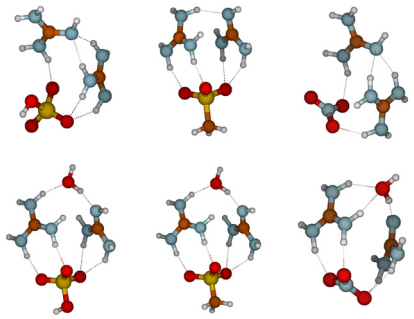

Fig. 4 Molecular structures of 1SA2GUA (left), 1MSA2GUA (middle), and 1NA2GUA clusters in their dry (top) and mono-hydrated (bottom) forms.

Interestingly, even at low relative humidity, 1SA2GUA, 1MSA2GUA, and 1NA2GUA clusters appear slightly more in hydrated than dry form. Fig. 4 shows the molecular structures of 1 acid–2 guanidine clusters without water and with one water molecule. In all clusters, the water molecule is located between the guanidine molecules, increasing the hydrogen bond angles, thus making the structure more relaxed. This structural relaxation is likely to explain the observed high hydration ability of those clusters, and perhaps this relaxation affects more the MSA than SA clusters which could explain the observed higher water absorption ability of MSA–GUA than SA–GUA clusters. Indeed, the Gibbs free energy of adding a water molecule to the 1MSA2GUA cluster is -5.2 kcal mol^{-1}, whereas for corresponding SA and NA, the reaction free energy is -4.1 and -4.2 kcal mol^{-1}, respectively.

4 Conclusions

The explicit role of relative humidity in NPF was explored by quantum chemical investigations and cluster dynamics simulations under atmospherically relevant conditions. Salt particles containing different acid molecules with guanidine were studied and it was found that SA–GUA and MSA–GUA clusters become hydrated with increasing RH which affects the cluster stabilities by up to five orders of magnitude. However, the effect on the NPF rates is very minor and the humidity factor varies mainly between 0.8 and 1.5. This is due to the high stability of the main cluster growth pathway (with or without water), and as the cluster evaporation is negligible, NPF can be said to occur at the kinetic limit.[21,39] In the case of MSA–GUA particle formation at high temperature, the humidity factor can be up to 300.

Nitric acid–guanidine clusters may uptake less water compared to SA and MSA clusters. The smallest hydrated clusters become stabilized against evaporation with increasing humidity, which enhances the formation of NA–GUA particles. Under ambient conditions relevant to the lower troposphere, the humidity factor in NA–GUA particle formation can be close to 10^4. Understanding the enhancing effect of water in nitric acid NPF is important to assess the impacts of nitrate aerosols on regulating the climate of the Earth. Nitric acid might be more important to the atmospheric NPF than previously thought, especially in the case of multi-compound NPF and high relative humidity.[56,61–63]

As shown in this study and in numerous previous studies, relative humidity has non-straightforward effects on the formation and evaporation rates of different acid–base clusters, and these effects might have complex temperature-dependence.[21,57,64] As it is not possible to compute hydration factors for all different acid–base combinations, further studies should focus to derive computationally cheap but accurate parametrization to compute hydration factors. Hydration parametrization for atmospheric NPF is essential to include the molecular-level effects of water in NPF in global climate modeling.

Conflicts of interest

There are no conflicts to declare.

Acknowledgements

NM acknowledges the Academy of Finland for funding (grant no. 347775) and the CSC-IT Center for Science in Espoo, Finland, for computational resources.

References

1 A. Jones, D. Roberts and A. Slingo, *Nature*, 1994, **370**, 450–453.
2 A. Gettelman and S. C. Sherwood, *Current climate change reports*, 2016, vol. 2, pp. 179–189.
3 D. Zhao, A. Buchholz, B. Kortner, P. Schlag, F. Rubach, A. Kiendler-Scharr, R. Tillmann, A. Wahner, J. Flores and Y. Rudich, *et al.*, *Geophys. Res. Lett.*, 2015, **42**, 10–920.
4 G. Almeida, J. Brito, C. Morales, M. D. F. Andrade and P. Artaxo, *Atmos. Chem. Phys.*, 2014, **14**, 7559–7572.
5 C. Randles, L. Russell and V. Ramaswamy, *Geophys. Res. Lett.*, 2004, **31**, L16108.
6 P. Zieger, O. Väisänen, J. C. Corbin, D. G. Partridge, S. Bastelberger, M. Mousavi-Fard, B. Rosati, M. Gysel, U. Krieger and C. Leck, *et al.*, *Nat. Commun.*, 2017, **8**, 1–10.
7 O. H. Berg, E. Swietlicki and R. Krejci, *J. Geophys. Res.: Atmos.*, 1998, **103**, 16535–16545.
8 K. A. Koehler, P. J. DeMott, S. M. Kreidenweis, O. B. Popovicheva, M. D. Petters, C. M. Carrico, E. D. Kireeva, T. D. Khokhlova and N. K. Shonija, *Phys. Chem. Chem. Phys.*, 2009, **11**, 7906–7920.
9 U. Lohmann, F. Friebel, Z. A. Kanji, F. Mahrt, A. A. Mensah and D. Neubauer, *Nat. Geosci.*, 2020, **13**, 674–680.
10 W. Y. Cheng, G. G. Carrió, W. R. Cotton and S. M. Saleeby, *J. Geophys. Res.: Atmos.*, 2009, **114**, D08201.
11 G. Feingold, W. L. Eberhard, D. E. Veron and M. Previdi, *Geophys. Res. Lett.*, 2003, **30**, 1287.
12 IPCC (Intergovernmental Panel on Climate Change), *Climate change* 2013: *The Physical Science Basis*, 2013.
13 J. Liu, F. Zhang, W. Xu, Y. Sun, L. Chen, S. Li, J. Ren, B. Hu, H. Wu and R. Zhang, *Geophys. Res. Lett.*, 2021, **48**, e2020GL091683.
14 X. Li, S. Chee, J. Hao, J. P. Abbatt, J. Jiang and J. N. Smith, *Atmos. Chem. Phys.*, 2019, **19**, 1555–1570.

15 A. Kürten, C. Li, F. Bianchi, J. Curtius, A. Dias, N. M. Donahue, J. Duplissy, R. C. Flagan, J. Hakala, T. Jokinen, J. Kirkby, M. Kulmala, A. Laaksonen, K. Lehtipalo, V. Makhmutov, A. Onnela, M. P. Rissanen, M. Simon, M. Sipilä, Y. Stozhkov, J. Tröstl, P. Ye and P. H. McMurry, *Atmos. Chem. Phys.*, 2018, **18**, 845–863.
16 S. Chee, K. Barsanti, J. N. Smith and N. Myllys, *Atmos. Chem. Phys.*, 2021, **21**, 11637–11654.
17 N. Myllys, T. Ponkkonen, M. Passananti, J. Elm, H. Vehkamäki and T. Olenius, *J. Phys. Chem. A*, 2018, **122**, 4717–4729.
18 N. Myllys, J. Kubecka, V. Besel, D. Alfaouri, T. Olenius, J. N. Smith and M. Passananti, *Atmos. Chem. Phys.*, 2019, **19**, 9753–9768.
19 Y. Liu, H.-B. Xie, F. Ma, J. Chen and J. Elm, *Environ. Sci. Technol.*, 2022, 7751–7760.
20 H. Henschel, T. Kurtén and H. Vehkamäki, *J. Phys. Chem. A*, 2016, **120**, 1886–1896.
21 T. Olenius, R. Halonen, T. Kurtén, H. Henschel, O. Kupiainen-Määttä, I. K. Ortega, C. N. Jen, H. Vehkamäki and I. Riipinen, *J. Geophys. Res.: Atmos.*, 2017, **122**, 7103–7118.
22 H. Chen, M. E. Varner, R. B. Gerber and B. J. Finlayson-Pitts, *J. Phys. Chem. B*, 2016, **120**, 1526–1536.
23 J. Kubecka, V. Besel, T. Kurtén, N. Myllys and H. Vehkamäki, *J. Phys. Chem. A*, 2019, **123**, 6022–6033.
24 J. Zhang and M. Dolg, *Phys. Chem. Chem. Phys.*, 2015, **17**, 24173–24181.
25 J. Zhang and M. Dolg, *Phys. Chem. Chem. Phys.*, 2016, **18**, 3003–3010.
26 C. Bannwarth, S. Ehlert and S. Grimme, *J. Chem. Theory Comput.*, 2019, **15**, 1652–1671.
27 J.-D. Chai and M. Head-Gordon, *Phys. Chem. Chem. Phys.*, 2008, **10**, 6615–6620.
28 R. Krishnan, J. S. Binkley, R. Seeger and J. A. Pople, *J. Chem. Phys.*, 1980, **72**, 650–654.
29 M. J. Frisch, G. W. Trucks, H. B. Schlegel, G. E. Scuseria, M. A. Robb, J. R. Cheeseman, G. Scalmani, V. Barone, G. A. Petersson, H. Nakatsuji, X. Li, M. Caricato, A. V. Marenich, J. Bloino, B. G. Janesko, R. Gomperts, B. Mennucci, H. P. Hratchian, J. V. Ortiz, A. F. Izmaylov, J. L. Sonnenberg, D. Williams-Young, F. Ding, F. Lipparini, F. Egidi, J. Goings, B. Peng, A. Petrone, T. Henderson, D. Ranasinghe, V. G. Zakrzewski, J. Gao, N. Rega, G. Zheng, W. Liang, M. Hada, M. Ehara, K. Toyota, R. Fukuda, J. Hasegawa, M. Ishida, T. Nakajima, Y. Honda, O. Kitao, H. Nakai, T. Vreven, K. Throssell, J. A. Montgomery, Jr., J. E. Peralta, F. Ogliaro, M. J. Bearpark, J. J. Heyd, E. N. Brothers, K. N. Kudin, V. N. Staroverov, T. A. Keith, R. Kobayashi, J. Normand, K. Raghavachari, A. P. Rendell, J. C. Burant, S. S. Iyengar, J. Tomasi, M. Cossi, J. M. Millam, M. Klene, C. Adamo, R. Cammi, J. W. Ochterski, R. L. Martin, K. Morokuma, O. Farkas, J. B. Foresman and D. J. Fox, *Gaussian16 Revision A.03*, 2016.
30 C. Riplinger and F. Neese, *J. Chem. Phys.*, 2013, **138**, 034106.
31 C. Riplinger, B. Sandhoefer, A. Hansen and F. Neese, *J. Chem. Phys.*, 2013, **139**, 134101.
32 C. Riplinger, P. Pinski, U. Becker, E. F. Valeev and F. Neese, *J. Chem. Phys.*, 2016, **144**, 024109.
33 R. A. Kendall, T. H. Dunning and R. J. Harrison, *J. Chem. Phys.*, 1992, **96**, 6796–6806.
34 D. G. Liakos, M. Sparta, M. K. Kesharwani, J. M. L. Martin and F. Neese, *J. Chem. Theory Comput.*, 2015, **11**, 1525–1539.
35 F. Neese, *Wiley Interdiscip. Rev.: Comput. Mol. Sci.*, 2012, **2**, 73–78.
36 N. Myllys, J. Elm, R. Halonen, T. Kurtén and H. Vehkamäki, *J. Phys. Chem. A*, 2016, **120**, 621–630.
37 N. Myllys, J. Elm and T. Kurtén, *Comput. Theor. Chem.*, 2016, **1098**, 1–12.
38 J. Elm, J. Kubecka, V. Besel, M. J. Jääskeläinen, R. Halonen, T. Kurten and H. Vehkamäki, *J. Aerosol Sci.*, 2020, **149**, 105621.
39 J. N. Smith, D. C. Draper, S. Chee, M. Dam, H. Glicker, D. Myers, A. E. Thomas, M. J. Lawler and N. Myllys, *J. Aerosol Sci.*, 2020, 105733.
40 M. J. McGrath, T. Olenius, I. K. Ortega, V. Loukonen, P. Paasonen, T. Kurtén, M. Kulmala and H. Vehkamäki, *Atmos. Chem. Phys.*, 2012, **12**, 2345–2355.
41 T. Olenius, O. Kupiainen-Määttä, I. K. Ortega, T. Kurtén and H. Vehkamäki, *J. Chem. Phys.*, 2013, **139**, 084312.
42 S. Chee, N. Myllys, K. C. Barsanti, B. M. Wong and J. N. Smith, *J. Phys. Chem. A*, 2019, **123**, 5640–5648.
43 M. Liu, N. Myllys, Y. Han, Z. Wang, L. Chen, W. Liu and J. Xu, *Front. Ecol. Evol.*, 2022, **10**, 324.
44 V. Loukonen, T. Kurtén, I. K. Ortega, H. Vehkamäki, A. A. H. Pádua, K. Sellegri and M. Kulmala, *Atmos. Chem. Phys.*, 2010, **10**, 4961–4974.
45 N. T. Tsona, H. Henschel, N. Bork, V. Loukonen and H. Vehkamäki, *J. Phys. Chem. A*, 2015, **119**, 9670–9679.
46 J. Elm, *J. Phys. Chem. A*, 2017, **121**, 8288–8295.
47 S.-H. Lee, H. Gordon, H. Yu, K. Lehtipalo, R. Haley, Y. Li and R. Zhang, *J. Geophys. Res.: Atmos.*, 2019, **124**, 7098–7146.
48 H. Chen and B. J. Finlayson-Pitts, *Environ. Sci. Technol.*, 2017, **51**, 243–252.
49 M. L. Dawson, M. E. Varner, V. Perraud, M. J. Ezell, R. B. Gerber and B. J. Finlayson-Pitts, *Proc. Natl. Acad. Sci. U. S. A.*, 2012, **109**, 18719–18724.
50 F. Eisele and D. Tanner, *J. Geophys. Res.: Atmos.*, 1993, **98**, 9001–9010.
51 H. Berresheim, F. Eisele, D. Tanner, L. McInnes, D. Ramsey-Bell and D. Covert, *J. Geophys. Res.: Atmos.*, 1993, **98**, 12701–12711.
52 G. Huang, X. Zhou, G. Deng, H. Qiao and K. Civerolo, *Atmos. Environ.*, 2002, **36**, 2225–2235.
53 B. Appel, S. Wall, Y. Tokiwa and M. Haik, *Atmos. Environ.*, 1967, **14**, 549–554.
54 V. Besel, J. Kubecka, T. Kurtén and H. Vehkamäki, *J. Phys. Chem. A*, 2020, **124**, 5931–5943.
55 H. Rodhe, P. Crutzen and A. Vanderpol, *Tellus*, 1981, **33**, 132–141.
56 L. Liu, H. Li, H. Zhang, J. Zhong, Y. Bai, M. Ge, Z. Li, Y. Chen and X. Zhang, *Phys. Chem. Chem. Phys.*, 2018, **20**, 17406–17414.
57 Y. Yang, S. E. Waller, J. J. Kreinbihl and C. J. Johnson, *J. Phys. Chem. Lett.*, 2018, **9**, 5647–5652.
58 S. E. Harold, C. J. Bready, L. A. Juechter, L. A. Kurfman, S. Vanovac, V. R. Fowler, G. E. Mazaleski, T. T. Odbadrakh and G. C. Shields, *J. Phys. Chem. A*, 2022, **126**, 1718–1728.

59 Y. Yang and C. J. Johnson, *Faraday Discuss.*, 2019, **217**, 47–66.
60 N. Myllys, D. Myers, S. Chee and J. N. Smith, *Phys. Chem. Chem. Phys.*, 2021, **23**, 13106–13114.
61 C. J. Bready, V. R. Fowler, L. A. Juechter, L. A. Kurfman, G. E. Mazaleski and G. C. Shields, *Environ. Sci.: Atmos.*, 2022, **2**, 1469–1486.
62 M. Wang, W. Kong, R. Marten, X.-C. He, D. Chen, J. Pfeifer, A. Heitto, J. Kontkanen, L. Dada and A. Kürten, *et al.*, *Nature*, 2020, **581**, 184–189.
63 L. Liu, F. Yu, L. Du, Z. Yang, J. S. Francisco and X. Zhang, *Proc. Natl. Acad. Sci. U. S. A.*, 2021, **118**, e2108384118.
64 J. J. Kreinbihl, N. C. Frederiks and C. J. Johnson, *J. Chem. Phys.*, 2021, **154**, 014304.